Final-focus systems in linear colliders

T. O. Raubenheimer and F. Zimmermann

Stanford Linear Accelerator Center, Stanford University, P.O. Box 4349, Stanford, California 94309

In colliding-beam facilities, the ''final-focus system'' must demagnify the beams to attain the very small spot sizes required at the interaction points. The first final-focus system with local chromatic correction was developed for the Stanford Linear Collider, where very large demagnifications were desired. This same conceptual design has been adopted by all of the future linear collider designs as well as the Superconducting Super Collider, the Stanford and KEK B Factories, and the proposed Muon Collider. In this paper, the overall layout, physics constraints, and optimization techniques relevant to the design of final-focus systems for high-energy electron-positron linear colliders are reviewed. Finally, advanced concepts to avoid some of the limitations of these systems are discussed.

CONTENTS

I. INTRODUCTION

Particle physics is an experimental science studying the fundamental forces and elementary particles that form the building blocks of our natural world. Most of the processes of interest become apparent at high energies. For this reason, most progress in our understanding of nature, from the atomic structure to the quarks and gluons inside a proton, has been made by colliding high-energy particles, usually protons and antiprotons, or electrons and positrons. For the past few decades, these particles were accelerated and collided in circular storage rings, the sole exception being the Stanford Linear Collider (SLC) (Seeman, 1990). In a storage ring, synchrotron radiation emitted by the bent electrons causes an energy loss per turn that, for constant bending radius, increases with the fourth power of the beam energy. Because this radiated energy must be replaced with a costly rf system, the radiation effectively limits the maximum energy of circular e^+/e^- storage rings. The largest circular collider ever built is the LEP ring in Geneva (Myers, 1995), which has a 30-km circumference with a beam energy close to 100 GeV.

It is generally assumed (Loew, 1995) that the generation of electron-positron colliders following the LEP must be linear colliders, with the SLC as a successful prototype. In a linear collider, the beams are accelerated in straight linear accelerators aimed at the collision point to reduce the synchrotron radiation problems. Instead of having the optimized cost increase as the energy squared, the cost of the linear collider is roughly proportional to the final energy. As an example of a future linear collider design, a schematic of the Next Linear Collider (NLC) being designed by a U.S. colllaboration, is illustrated in Fig. 1. The linear collider complex consists of two roughly equivalent halves, which are aimed at each other. Each half is composed of an injector complex for beam generation, a damping ring which improves the beam quality, a linear accelerator in which the beam gains the desired energy, a collimation system which removes the beam halo that otherwise could cause background in the particle-physics detector, a final-focus system, and the collision point, followed on the other side by an exit line for the spent beam.

Although linear colliders avoid the limitation due to synchrotron radiation in a storage ring, there are other problems, namely, accelerating the beams and producing the very small spot sizes that are necessary at the interaction point. The small spot sizes are necessary to achieve reasonable reaction rates because the reaction rate is given by the process cross section, which tends to decrease with the square of the center-of-mass energy, multiplied by the collider luminosity. Assuming Gaussian beams and head-on collisions, the collider luminosity can be written

$$\mathcal{L} \approx \frac{f_{rep}}{2\pi} \frac{n_b N_+ N_-}{\Sigma_x^\star \Sigma_y^\star}, \tag{1}$$

where f_{rep} is the collider repetition rate, n_b is the number of bunches per pulse, $N_\pm$ is the number of particles per bunch, and $\Sigma_{x,y}^\star$ are the sums in quadrature of the rms horizontal and vertical sizes of the colliding beams, i.e., $\Sigma_x^\star = \sqrt{\sigma_{x1}^{\star 2} + \sigma_{x2}^{\star 2}}$ and $\Sigma_y^\star = \sqrt{\sigma_{y1}^{\star 2} + \sigma_{y2}^{\star 2}}$, where $\sigma_{x,y\,1}^\star$ and $\sigma_{x,y\,2}^\star$ denote the single-beam rms spot sizes of the two beams.

Unlike a storage ring, a linear collider collides the high-energy beams only once, and the beams must be

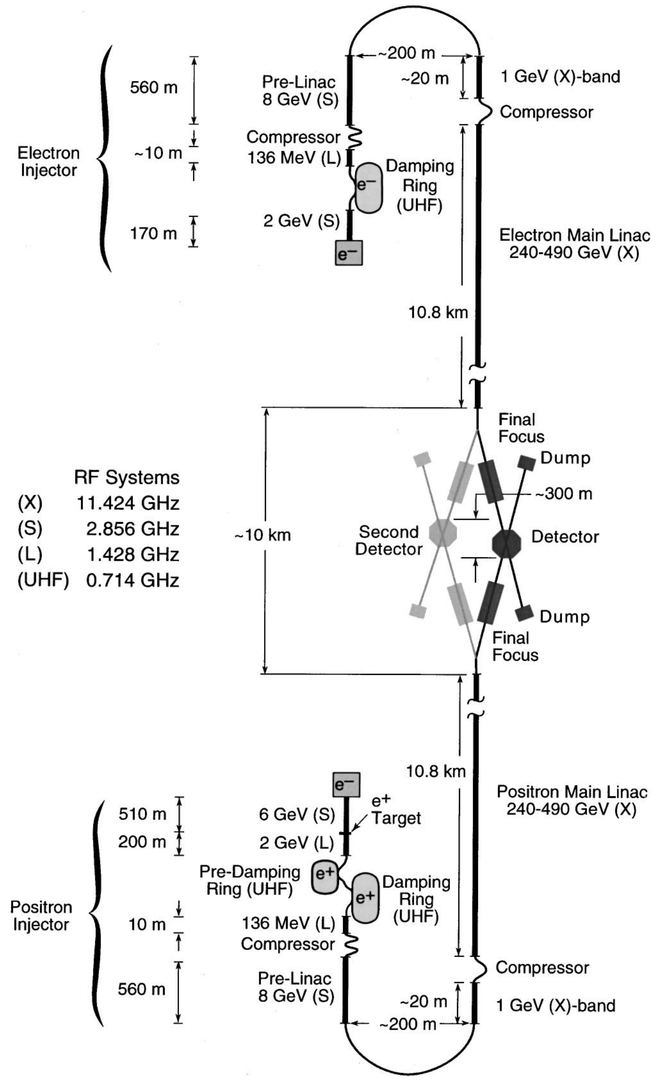

FIG. 1. Schematic of the Stanford Next Linear Collider, a future 1-TeV linear collider.

regenerated at each pulse. In view of technological limits on the linear-accelerator repetition rate, and in order to constrain the power consumption of the collider, the collision frequency f_{rep} is two or three orders of magnitude smaller than in a storage ring. Thus, to attain comparable luminosity, the linear colliders accelerate long trains of bunches and focus them to very small spot sizes. Fortunately, because the beams are not collided again, the minimum spot size is not limited by the beam-beam tune shift as it is in a circular collider. However, the small spot sizes impose severe constraints on the final-focus system of the linear collider. For example, in the next generation of linear colliders, the collision spot size is measured in nanometers; parameters of a few circular and linear colliders are compared in Table I.

The horizontal and vertical rms beam sizes, σ_x and σ_y, at location s can be expressed as

$$\sigma_x(s)=\sqrt{\beta_x\epsilon_x} \tag{2}$$

$$\sigma_y(s)=\sqrt{\beta_y\epsilon_y}, \tag{3}$$

where $\epsilon_{x,y}$ denotes the horizontal or vertical emittance and $\beta_{x,y}(s)$ is the horizontal or vertical beta function. In the absence of acceleration and synchrotron radiation, the emittance is an invariant quantity, measuring the area in phase space occupied by the beam. The beta function characterizes the variation of the beam envelope as a function of s. Both emittance and beta function are quoted in units of length. A star is used to designate variables at the collision point. For example, $\sigma_y^\star$ is the vertical rms beam size and $\beta_y^\star$ the vertical beta function at the collision point.

The purpose of the final-focus system (FFS) in a linear collider is to demagnify the beams to the very small spot sizes required at the interaction point. In principle, the FFS operates as a simple telescope. However, the strong focusing quadrupoles that produce the small spots also generate very large chromaticities. Thus to focus a beam with a finite energy spread, the system must be chromatically corrected. The normal procedure is to perform the chromatic correction by placing sextupole magnets in regions of dispersion where pairs of sextupoles are separated by 180° in the betatron phase, so that the geometric aberrations cancel. More precisely, the optical transport or R matrix (Brown, 1968), which relates transverse positions (x and y) and slopes ($x'\equiv dx/ds$ and $y'\equiv dy/ds$, where s is the position along the beam line) of particle trajectories at the first and second sextupole, is a $-I$ transform:

$$\begin{pmatrix} x \\ x' \\ y \\ y' \end{pmatrix}_2 = \begin{pmatrix} -1 & 0 & 0 & 0 \\ 0 & -1 & 0 & 0 \\ 0 & 0 & -1 & 0 \\ 0 & 0 & 0 & -1 \end{pmatrix} \begin{pmatrix} x \\ x' \\ y \\ y' \end{pmatrix}_1 . \tag{4}$$

The subindices 1 or 2 refer to the coordinates at the first and second sextupole.

However, even if separated by a $-I$, the sextupoles introduce higher-order geometric and chromogeometric

TABLE I. Parameters of a few linear colliders (SLC and NLC) and circular colliders (PEP-II and LEP). Listed for each are the repetition rate, the number of bunches per train (n_b), the number of particles per bunch (N), and the rms transverse beam sizes at the collision point ($\sigma_x^\star$ and $\sigma_y^\star$).

	Luminosity	$f_{\rm rep}$	n_b	$N[10^{10}]$	$\sigma_x^\star$ [μm]	$\sigma_y^\star$ [μm]
NLC	1×10^{34}	120 Hz	90	1	0.25	0.004
SLC	2×10^{30}	120 Hz	1	4	1.5	0.5
PEP-II	3×10^{33}	140 kHz	1700	4	155	6
LEP2	5×10^{31}	10 kHz	8	30	240	4

aberrations that may have to be controlled by careful placement of the elements or additional multipole magnets. It should be noted that similar chromatic cancellation techniques for the final focus were adopted for the Superconducting Super Collider, the Stanford and KEK B Factories, and the proposed Muon Collider.

In most linear-collider designs, the interaction-point spots are asymmetric: the vertical spot size is much smaller than the horizontal; this maximizes the luminosity while minimizing the beam-beam interaction and easing the constraints on the final focus. Typical designs have a demagnification of a few hundred in the vertical plane with an order of magnitude less in the horizontal. The vertical focusing is usually set close to the limit from the depth of focus, i.e., $\beta_y \sim \sigma_z$, where σ_z is the rms bunch length, but other constraints, such as the chromaticity or tolerances on the components, may lead to a weaker optimal choice. In the following, we shall describe the basic layout of a final-focus system and then discuss many of the limitations that must be considered in the design. Finally, we shall describe some of the design and optimization techniques that are important and some of the more advanced concepts that have been proposed. Throughout this article, we shall ignore many of the more design-specific issues, such as detailed tolerance calculations, collimation, masking, and machine protection. Detailed discussions of all the relevant effects can be found in any of the future linear-collider design documents (Raubenheimer *et al.*, 1996; Akasaka *et al.*, 1997; Brinkmann *et al.*, 1997) or in the work of Roy (1992), which discusses the design of the Final Focus Test Beam (FFTB) at Stanford. Many of the detailed expressions used in this note originate in Raubenheimer *et al.* (1996) and in the review of Roy (1992).

II. LAYOUT

The first linear collider FFS in operation was that at the Stanford Linear Collider (SLC) (Brown and Spencer, 1981; Murray *et al.*, 1987). To save space, the SLC final focus was designed with an interleaved horizontal and vertical chromatic correction section. Unfortunately, the interleaved sextupoles introduce higher-order aberrations. While these aberrations are not a severe limitation in the SLC, they would be in systems with greater demagnification.

To limit the high-order aberrations, most of the next-generation final-focus systems have been designed in a modular manner with separate sections for horizontal and vertical chromaticity correction. Thus a typical final-focus system consists of a beta-matching section to adjust the final focus for the incoming beam, a diagnostic region to verify the incoming beam properties, a horizontal chromaticity correction section (CCX), a beta exchange region (BX), a vertical chromaticity correction section (CCY), a final transformer, and the final lens, which is usually a quadrupole doublet. Figure 2 illustrates the optics in the Final-Focus Test Beam (FFTB) at Stanford (Berndt *et al.*, 1991), which is a model for the final focus in a future linear collider.

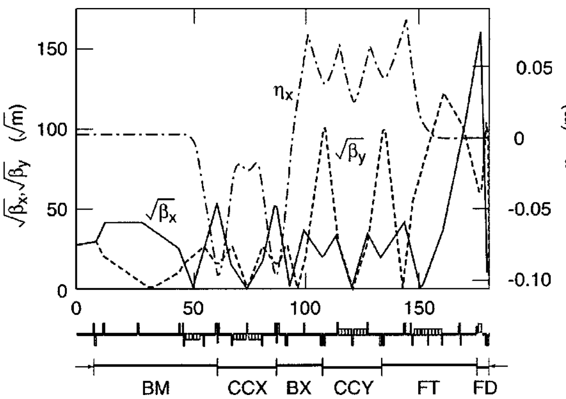

FIG. 2. Schematic of the final-focus system of the Final-Focus Test Beam at Stanford: BM, beta-matching section; CCX, horizontal chromaticity correction section; BX, beta-exchange region; CCY, vertical chromaticity correction section; FT, final transformer; FD, final-doublet lens. From Berndt *et al.*, 1991.

Most next-generation linear-collider designs operate with long trains of bunches to make more efficient use of the rf systems. When these bunches are closely spaced, the final-focus systems are designed with beam trajectories intersecting at a "crossing angle" Θ_c at the interaction point. This avoids any parasitic bunch collisions and provides a method of separating the incoming and outgoing beams so that the latter can be directed to the beam dumps. Unfortunately, this crossing angle will reduce the luminosity unless the beams are "crabbed," i.e., tilted in x-z space so that they pass through each other head on.

III. LUMINOSITY

The luminosity in a linear collider can be expressed as (Chen and Yokoya, 1992)

$$\mathcal{L} = \mathcal{L}_0 \tilde{H}_D = \mathcal{L}_{00} H_D . \tag{5}$$

Here, H_D or $\tilde{H}_D$ characterizes the luminosity enhancement, which depends upon the beam-beam interaction and is discussed in Sec. IV; $\mathcal{L}_{00}$ is the ideal luminosity for a head-on collision and zero bunch length; and $\mathcal{L}_0$ is the geometric luminosity, including the effect of a finite bunch length and the depth of focus. The luminosity $\mathcal{L}_0$ depends on the beam properties as well as the FFS properties such as the depth of focus and the (horizontal) bunch crossing angle θ_c; note that with perfect crab crossing $\theta_c = 0$, while without crab crossing $\theta_c = \Theta_c$, the angle at which the trajectories cross.

The ideal short-bunch luminosity is

$$\mathcal{L}_{00} = \frac{f_{rep} n_b N^2}{4\pi \sigma_x^\star \sigma_y^\star} \tag{6}$$

and the actual geometric luminosity can be expressed as

$$\mathcal{L}_0 = \mathcal{L}_{00}\, \eta(C_\theta, A_y), \tag{7}$$

where f_{rep}, n_b, and N are the repetition rate, the number of bunches per pulse, and the bunch charge, respectively. In addition, $\sigma^\star_{x,y}$ are the rms beam sizes at the interaction point and η describes the effects due to depth of focus and the crossing angle. Assuming flat Gaussian beams ($\sigma_x \gg \sigma_y$), η can be written

$$\eta(C_\theta, A_y) = \frac{1}{A_y\sqrt{\pi}} e^x K_0(x), \quad x \equiv \frac{1+C_\theta^2/4}{2A_y^2}, \tag{8}$$

where K_0 is the modified Bessel function, $A_y \equiv \sigma_z/\beta_y^\star$ describes the depth of focus, and $C_\theta \equiv \theta_c \sigma_z/\sigma_x$ is the ratio of the bunch diagonal angle to the bunch crossing angle θ_c. The geometric luminosity loss is about 14% when $A_y=1$ and is another 10% when $C_\theta=1$. Typically, final-focus systems are designed with $A_y \lesssim 1$ and $C_\theta \lesssim 1$. Techniques have been developed or proposed for reducing the sensitivity to the crossing angle, discussed in Sec. V, and the sensitivity to the depth of focus, which will be discussed in Sec. XIII.

IV. BEAM-BEAM INTERACTION

Excellent reviews of the beam-beam effects in linear colliders are available (Chen and Yokoya, 1988a, 1992). In the following we summarize some of the main features.

The collision strength at a linear collider is measured in terms of the horizontal and vertical parameters,

$$D_{x,y} = \frac{2Nr_e\sigma_z}{\gamma\sigma_{x,y}^\star(\sigma_x^\star + \sigma_y^\star)}, \tag{9}$$

where N denotes the number of particles per bunch, γ the relativistic Lorentz factor, and r_e the classical electron radius. In linear approximation, the number of oscillations a particle undergoes in the field of the opposing beam is $\sim \sqrt{\sqrt{3}D_{x,y}}/(2\pi)$. The parameter D is called the disruption parameter and is the equivalent of the beam-beam tune-shift parameter in a ring collider (the two quantities are identical in the case $\beta^\star \approx \sigma_z$). Values for D can vary between 1 (SLC) and almost 10 (Next Linear Collider).

During the collision, particles emit synchrotron radiation in the field of the opposing beam. This radiation is called beamstrahlung, and it is characterized by the Υ parameter, which is proportional to the average critical energy,

$$\Upsilon = \frac{2\hbar\omega_c}{3E} \approx \frac{5}{6}\frac{\gamma r_e^2 N}{\alpha\sigma_z(\sigma_x+\sigma_y)}, \tag{10}$$

where $\alpha \approx 1/137$ is the fine-structure constant, $\omega_c \equiv 3c\gamma^3/(2\rho)$ is the critical frequency characterizing the synchrotron light spectrum, with ρ the local bending radius, γ is the Lorentz factor, c is the speed of light (Sands, 1979), and σ_z is the rms bunch length. Coherent pair creation becomes the prevailing source of background for Υ above 0.5, a regime avoided in most collider designs.

The number of beamstrahlung photons emitted per electron is

$$N_\gamma \approx \frac{5\alpha\sigma_z}{2\gamma\lambda\!\!\!^{-}_e}\frac{\Upsilon}{(1+\Upsilon^{2/3})^{1/2}} \approx 2\frac{\alpha r_e N}{\sigma_x+\sigma_y}, \tag{11}$$

where $\lambda\!\!\!^{-}_e$ is the electron Compton wavelength [$\lambda\!\!\!^{-}_e = \hbar/(m_e c)$], and the last approximation applies if Υ is small ($\Upsilon \lesssim 1$). The number N_γ should not be much larger than 1 for background considerations. The fraction of the luminosity at the design center-of-mass energy is given by $\Delta\mathcal{L}/\mathcal{L} \approx 1/N_\gamma^2(1-e^{-N_\gamma})^2$, and the average relative energy loss due to beamstrahlung is

$$\delta_B \approx \frac{1}{2}N_\gamma\Upsilon = \frac{r_e^3 N^2\gamma}{\sigma_z\sigma_x^2(1+\sigma_y/\sigma_x)^2}. \tag{12}$$

The three quantities Υ, N_γ, and δ_B can be reduced by operating with (1) flat beams and (2) long bunches, or by more exotic approaches such as (3) charge compensation (Balakin and Solyak, 1986; Rosenzweig *et al.*, 1989) or (4) a plasma at the interaction point (Whittum *et al.*, 1990).

In terms of N_γ, the luminosity for a flat-beam linear collider may be rewritten as

$$L \approx \left(\frac{5}{r_e}\right)\frac{P_{wall}}{E_{beam}} N_\gamma \frac{\eta}{\sigma_y}, \tag{13}$$

where P_{wall} is the wall-plug power (i.e., the electrical power required to operate the collider), and $\eta = P_{beam}/P_{wall}$ is the ratio of beam power to wall-plug power (efficiency). If N_γ and the energy are held constant, the luminosity can be raised only by increasing the power-conversion efficiency and by reducing the vertical spot size.

Due to the attraction of the colliding particles by the other beam, the effective beam size at the interaction point is smaller and the luminosity is higher by a factor of $H_D = \mathcal{L}/\mathcal{L}_{00}$ than it would be without the collision. This so-called pinch effect (Hollebeek, 1981) is significant for disruption parameters $D_{x,y}$ larger than 1.

An empirical formula of the pinch enhancement for head-on round-beam collisions, which was obtained by fitting a large number of simulation results, is (Chen and Yokoya, 1988a)

$$H_D^{round} \approx 1 + D^{1/4}\left(\frac{D^3}{1+D^3}\right)\left\{\ln(\sqrt{D}+1) + 2\ln\left(\frac{0.8}{A}\right)\right\}, \tag{14}$$

where $D = D_x = D_y$ and $A = \sigma_z/\beta_{x,y}^\star$. This formula for the factor H_D includes the effect of the depth of focus.

For flat beams or nearly flat beams, it was both shown in simulations (Chen and Yokoya, 1992; Chen, 1993) and expected on theoretical grounds (Rosenzweig and Chen, 1991) that

$$H_D^{flat} \approx (H_{Dx}^{round})^{1/2}(H_{Dy}^{round})^{f(R)}, \tag{15}$$

where H_{Dx} equals H_D^{round} as given in Eq. (14) with $D = D_x$, H_{Dy} equals H_D^{round} with $D = D_y$, and

$$f(R) = \frac{1+2R^3}{6R^3}, \tag{16}$$

where $R \equiv \sigma_x^\star/\sigma_y^\star$.

V. CROSSING ANGLE AND CRAB CROSSING

As mentioned above, a crossing angle is frequently used to separate the incoming and outgoing beams in a

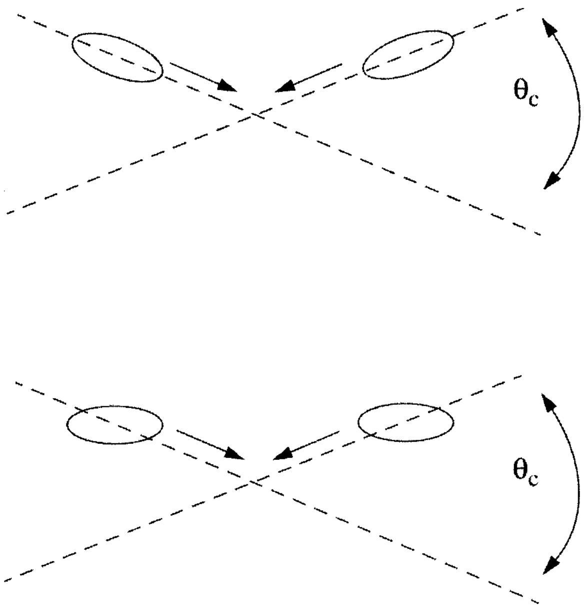

FIG. 3. Schematic of "uncrabbed" (top) and "crabbed" (bottom) collision with crossing angle.

long train of bunches. We shall address four primary issues with respect to a crossing angle. The first is simply geometry. The crossing angle needs to be sufficiently large to separate the beams and to provide a passage for the outgoing beam to escape the interaction region. If the crossing angle is large, it may be possible to have separate quadrupoles for the incoming and outgoing beams, while for a small crossing angle an exit port is usually needed in the final-doublet quadrupoles.

Second, a multibunch crossing instability (Chen and Yokoya, 1988b) can arise from parasitic bunch interactions. Assuming flat beams, the criterion for avoiding significant vertical displacement of the bunches due to this instability can be expressed as

$$(m_b-1) \ll \frac{C_\Theta^2}{D_x D_y}\sqrt{\frac{1}{2}+\frac{D_y}{3}}, \tag{17}$$

where $D_{x,y}$ are the disruption parameters discussed in Sec. IV and $C_\Theta = \Theta_c \sigma_z / \sigma_x$ (Θ_c is the trajectory crossing angle); C_Θ is not necessarily the same as C_θ, the bunch crossing angle, which was defined in Sec. III. In addition, m_b is the number of bunches that interact in the free space around the interaction point, which, assuming no additional masking, is $m_b = 1 + 2L^\star/\Delta_b$, where Δ_b is the bunch spacing and $L^\star$ is the free distance between the end of the last focusing quadrupole and the interaction point. This instability decreases rapidly with larger crossing angles.

Third, if the geometric luminosity loss due to the crossing angle, Eq. (7), is significant, i.e., when the trajectory crossing angle Θ_c is large compared to the bunch diagonal angle ($C_\Theta \gtrsim 1$), the beam can be crabbed (Palmer, 1998). Here the bunches are given a time-dependent horizontal position offset so that they collide head-on: $dx^\star/dz = \Theta_c/2$ (z is the longitudinal coordinate along the bunch), as is illustrated in Fig. 3.

There are two approaches to establish the crabbing: either use an rf-deflecting cavity or use the correlated energy spread along the bunch and a small amount of residual dispersion at the interaction point (Brinkmann, 1993). In the latter approach, the required dispersion is

$$\eta_x^\star \frac{\sigma_{\epsilon_c}}{\sigma_z} = \frac{\Theta_c}{2}, \tag{18}$$

where σ_{ϵ_c} is the correlated component of the rms energy spread, and $\eta_x^\star$ is the horizontal dispersion function at the collision point. The dispersion characterizes the shift in horizontal position as a function of beam energy: $\Delta x = \eta_x \delta$ (with δ the relative energy deviation). Its value at the interaction point is limited by the increase of the interaction-point spot size due to incoherent energy spread within the bunch.

In the case of a crab cavity, the required rf voltage is

$$V_{rf} = \frac{\Theta_c E \lambda_{rf}}{4\pi R_{12}}, \tag{19}$$

where E is the beam energy, R_{12} is the transport matrix element from the crab cavity to the interaction point (the R_{12} matrix element between two locations expresses a displacement Δx at the second location in terms of the kick θ imposed at the first one: $\Delta x = R_{12}\theta$), and λ_{rf} is the rf wavelength of the crab cavity. With a fully crabbed beam, the beam crossing angle θ_c is zero even though the trajectories intersect at an angle.

In general, the tolerances on the alignment and stability of the crab cavity are relatively loose. The exception is the relative phase tolerance between the crab cavities on either side of the interaction point. A phase difference between the cavities will cause a horizontal offset between the beams. To limit the luminosity dilution to 2%, the bunch separation must be less than $0.3\sigma_x$ rms. This imposes an rms tolerance on the phase difference between the cavities of

$$\Delta\phi_{rf} = 2\pi \frac{0.6\sigma_x}{\Theta_c \lambda_{rf}} \ \text{[radians]}. \tag{20}$$

Note that the tolerance on the bunch timing is much looser and just shifts the longitudinal interaction-point position with a luminosity loss that depends on the depth of focus.

Fourth, with a crossing angle, the beams do not travel parallel to the axis of the solenoidal field. For a horizontal crossing angle, this results in vertical deflections of the beams and, perhaps more importantly, in vertical dispersion at the interaction point. To estimate the effect, we shall assume that the final-doublet quadrupoles are outside of the solenoidal field. In this case, the vertical offset at the interaction point is

$$\Delta y^\star = \frac{B_s L^{\star 2}}{B\rho} \frac{\Theta_c}{4}, \tag{21}$$

where B_s is the solenoidal field and $B\rho$ is a function of the beam energy: in units of Tesla meters, $B\rho = 3.3356\, E[\text{GeV}]$. This deflection can be corrected by steering, but it is more difficult to correct the dispersion introduced by the deflection.

VI. OPTICAL ABERRATIONS

Almost all the aberrations in a FFS arise from the need to correct the chromaticity introduced by the final doublet:

$$\xi_y^\star \equiv \frac{L_y^c}{\beta_y^\star} = -\int ds K_1 \beta_y \approx -\frac{1}{\beta_y^\star}\int ds K_1 R_{34}^2, \tag{22}$$

where K_1 is the normalized quadrupole strength in units of m^{-2}, R_{34} is the (3,4) transport matrix element from position s to the interaction point, which relates an angular deflection to a position shift $\Delta y = R_{34}\Delta y'$, and the approximate relation is valid because the final doublet is $\sim 90°$ in betatron phase from the interaction point. The quantity L_y^c is the vertical chromatic length that, for a final doublet in which the final quadrupole is vertically focusing, can be limited to be only slightly larger than the free distance from the interaction point to the first quadrupole $L^\star$. This is in contrast to the horizontal chromatic length L_x^c, which tends to be much larger than $L^\star$, although in a flat-beam FFS, where $\beta_x^\star \gg \beta_y^\star$, the horizontal chromaticity is much smaller than the vertical.

If uncorrected, the chromaticity will lead to an energy-dependent increase in the spot size:

$$\frac{\Delta\sigma_{x,y}}{\sigma_{x,y}} \approx \xi_{x,y}\sigma_\epsilon, \tag{23}$$

to be added in quadrature, where σ_ϵ is the rms energy spread in the beam.

As mentioned, the chromaticity is corrected by placing sextupole magnets, located $n\pi$ in betatron phase from the final doublet, in regions of dispersion and large beta functions. The total integrated sextupole strength k_2 can be estimated from the need to compensate for the final-doublet chromaticity:

$$\text{CCX:}\quad k_2\eta_x\beta_x \approx \xi_x^\star \quad\text{and}\quad \text{CCY:}\quad k_2\eta_x\beta_y \approx -\xi_y^\star, \tag{24}$$

where we have assumed that the β_y is small in the CCX while the β_x is small in the CCY, so that there is little effect of one on the other.

The third-order geometric aberrations due to the sextupoles are canceled by separating the magnets by a $-I$ transformation, but there are still other optical aberrations that can be important. In particular, the chromatic sensitivity of the lattice providing the $-I$ transform between the sextupoles introduces third-order chromaticity and other fourth-order chromogeometric aberrations (Irwin, 1990). Some of these can be compensated for by using additional sextupoles placed throughout the final focus (Brinkmann, 1990) or by a nonsymmetric dispersion function in the chromatic correction sections (Oide, 1992). In the present generation of final-focus systems, the chromatic aberrations are canceled to fourth order or higher. This leads to a momentum bandwidth that is limited by very-high-order aberrations and causes a roughly rectangular aperture, as is illustrated in Fig. 4.

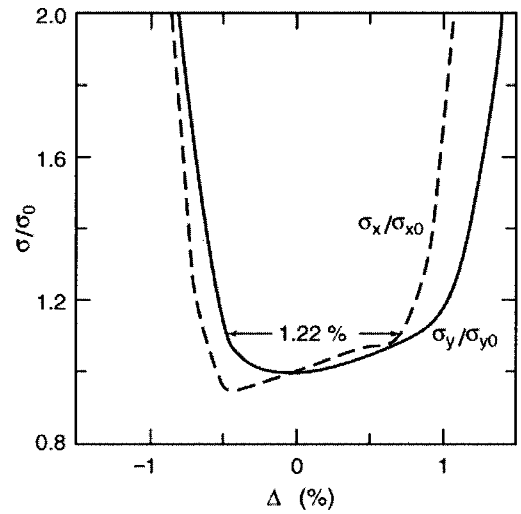

FIG. 4. Example of the energy bandwidth in a final-focus system (Raubenheimer *et al.*, 1996).

In addition, there are usually other, purely geometric, aberrations. One example arises from the finite sextupole length, which creates octupole-like fourth-order aberrations. For a given sextupole strength and length, the vertical spot size increase due to this aberration is (Roy, 1992)

$$\frac{\Delta\sigma_y^\star}{\sigma_y^\star} = k_2^2 L_s \beta_y^2 \epsilon_y \sqrt{\frac{5}{12} + \frac{\sigma_x^2}{6\sigma_y^2} + \frac{\sigma_x^2}{12\sigma_y^2}}, \tag{25}$$

where $\Delta\sigma^\star/\sigma^\star$ is added in quadrature to the unperturbed spot size, the beta functions and beam sizes are evaluated at the sextupole locations, L_s is the sextupole length, ϵ_y is the vertical emittance, and k_2 is the integrated sextupole strength in units of m^{-2}; a similar expression exists for the aberration in the horizontal plane and is found simply by switching the x and y indices.

VII. SYNCHROTRON RADIATION

Synchrotron radiation in the bending magnets that produce the dispersion in the CCX and CCY has two effects: first, it will enlarge the horizontal spot size and divergence (i.e., the horizontal emittance) due to the nonzero dispersion in these locations and, second, the change in the particle energy due to the radiation is not chromatically corrected. The first effect can be estimated (Sands, 1985; Roy, 1992):

$$\Delta\sigma_x^2 = CE^5 \int ds |G^3| (R_{16}^{s\to IP})^2, \tag{26}$$

$$\Delta\sigma_{x'}^2 = CE^5 \int ds |G^3| (R_{26}^{s\to IP})^2, \tag{27}$$

where $C = 4.13\times10^{-11}\,\mathrm{m}^2\,\mathrm{GeV}^{-5}$, G is the inverse of the local bending radius, and $R_{i6}^{s\to IP}$ is the $(i,6)$ R-matrix element from location s to the interaction point ($i = 1,2$), where the $R_{16}(s)$ and $R_{26}(s)$ matrix elements specify the effect of an energy error induced at location s on horizontal interaction-point position and slope, respectively. The prime refers to the slope of the trajectories, and thus $\Delta\sigma_{x'}$ is a contribution to the rms divergence. Note that the FFS can be rematched to account for the change in the beam phase-space orientation, which may result in a smaller luminosity loss than estimated from the above equations. The rematching usually requires reducing $\beta^\star$ by an amount comparable to the emittance dilution and is performed empirically by optimizing the interaction-point beam divergence.

The second effect can be estimated using the chromaticity of the final doublet:

$$\frac{\Delta\sigma_{x,y}}{\sigma_{x,y}} \approx \Delta\sigma_\epsilon \Delta\xi_{x,y}, \tag{28}$$

where $\Delta\xi$ is the uncorrected chromaticity, which is nominally zero upstream of the chromatic correction sections and is equal to $\xi^\star$ downstream of the chromatic correction sections. In addition, σ_ϵ is the rms energy spread, which can be expressed as

$$(\Delta\sigma_\epsilon)^2 = CE^5 \int ds |G^3|, \tag{29}$$

with all quantities defined above.

Another effect due to synchrotron radiation, referred to as the Oide effect, arises in the final lens when the radiation changes the particle's energy and this interacts with the local chromaticity (Oide, 1988). The effect depends on fields seen by the beam in the final quadrupoles, which is a function of both the horizontal and vertical extent of the beam. In the original reference, the horizontal beam size was ignored and the change in the rms spot size was found to be

$$(\Delta y^\star)^2 = \frac{110 r_e ƛ_e \gamma^5 \sigma_{y'}^{\star 5}}{3\sqrt{6\pi}} \int ds L_y^{c2} R_{34}^3 |K_1|^3, \tag{30}$$

where L_y^c is the chromatic length, defined in Eq. (22), and $ƛ_e$ is the Compton wavelength.

An approximate expression can be found including the horizontal beam size [Eq. (11.111) in Raubenheimer *et al.*, 1996]:

$$(\Delta y^\star)^2 \approx 1.22 r_e ƛ_e \gamma^5 \sigma_{y'}^{\star 2} \int ds L_y^{c2} |K_1|^3 (7\sigma_{y'}^{\star 2} R_{34}^2 + \sigma_{x'}^{\star 2} R_{12}^2) \sqrt{\sigma_{y'}^{\star 2} R_{34}^2 + \sigma_{x'}^{\star 2} R_{12}^2}. \tag{31}$$

However, the additional contribution from σ_x can be made relatively small by decreasing the strength of the horizontally focusing magnet in the final doublet.

Finally, it is important to note that even though the rms increase of the spot size due to the Oide effect can be significant, the probability of radiating photons in the final doublet is rather small and thus the resulting beam has an unperturbed core with large tails (Hirata *et al.*, 1989). Thus the actual luminosity decrease is much less than that naively calculated from the above expressions; for details the reader is referred to Hirata *et al.* (1989).

VIII. WAKE FIELDS

Wake fields can potentially be dangerous in the FFS because the beta functions are large, which makes the beam sensitive to the transverse deflections. In addition, the final-doublet chromaticity is large, which makes the beam very sensitive to any longitudinal wakefields between the CCY and the final doublet; an estimate of the tolerance on the induced energy spread can be made using Eq. (22). Both problems can be compounded by the need for collimators and protection masks, which are sometimes placed close to the beam. Thus, when designing a FFS, care must be taken to verify the wake fields of the components in the beam line; examples of such analyses for the SLC and Next Linear Collider final-focus systems are presented by Zimmermann *et al.* (1996) and Raubenheimer and Zimmermann (1996).

In addition to wake fields from the collimators and upstream elements, there are transverse geometric and resistive wake fields that can be important in the final doublet and in the chromatic correction sections, where the beta functions are very large. These wake fields will have two effects: they will increase the beam emittance and they will amplify any centroid jitter; we shall discuss the centroid jitter, since it imposes a more restrictive constraint. The centroid jitter amplification due to the resistive wall wake field is

$$\frac{\Delta y^\star}{\sigma_y^\star} = 1.6 \frac{N r_e}{\gamma\sigma_z} \frac{L\beta_{FD}\delta_s}{g^3} \left(\frac{\Delta y}{\sigma_y}\right)_{FD}, \tag{32}$$

where L is the length of the aperture, g is the beam-pipe radius, β_{FD} is the beta function in the final doublet, and $\delta_s = \sqrt{\sigma_z / Z_0 \sigma}$ is the skin depth of the beam pipe.

Similarly, the effect of a gentle taper can be estimated as (Yokoya, 1988)

$$\frac{\Delta y^\star}{\sigma_y^\star} = 0.56 \frac{N r_e}{\gamma\sigma_z} \frac{L\Theta^2\beta_{FD}}{g_1 g_2} \left(\frac{\Delta y}{\sigma_y}\right)_{FD}, \tag{33}$$

where L and Θ are the length and angle of the taper and g_1 and g_2 are the initial and final beam-pipe radii. Fortunately, both of these tolerances depend strongly on the beam-pipe radius and thus the effect can be minimized easily.

IX. SCATTERING

A distinct advantage of an electron-positron collider as compared with hadron colliders is the cleanliness of the events seen by the particle-physics detector. Preservation of this cleanliness imposes severe constraints on the acceptable detector background. Indeed, at both the SLC and at LEP, the ultimate luminosity was limited by detector background due to beam tails, which prevented further decreases in $\beta_{x,y}^\star$. Correct assessment of all background sources is thus essential in order to obtain the optimal luminosity in a future linear collider.

Particles that exceed a certain transverse amplitude or energy are lost in the final-focus region. When they impinge on a collimator or vacuum chamber, these electrons (or positrons) can generate muons penetrating through the detector. In addition, electrons that hit the final doublet may give rise to electromagnetic showers into the detector elements. Finally, particles passing the final-doublet quadrupoles at large transverse amplitudes emit synchrotron radiation, which can be another important background source.

The Next Linear Collider design adopted the criterion that fewer than ten electrons per bunch train (10^{12} particles) should hit the final doublets, and that fewer than 1 muon per bunch train should pass through the detector (Hertzbach *et al.*, 1996; Raubenheimer *et al.*, 1996). Because of extensive upstream collimation, scattering process in the final focus itself are a primary source of particle loss.

There are three scattering processes that are important: inelastic (bremsstrahlung) and elastic scattering on the residual gas atoms and scattering on the thermal photons. The bremsstrahlung and the scattering on thermal photons result in an energy loss of the scattered particle, while Coulomb scattering on the residual gas causes a change in the transverse oscillation amplitude.

The cross section for bremsstrahlung at high energies (assuming complete screening) is (Bethe and Ashkin, 1953)

$$\sigma_{brem} \approx \frac{16}{3} \alpha Z(Z+1.35) r_e^2 \ln\left(\frac{183}{Z^{1/3}}\right) \times \left[\ln\left(\frac{\delta_{max}}{\delta_{min}}\right) + \delta_{min} - \delta_{max}\right], \tag{34}$$

where α is the fine-structure constant, δ_{min} and δ_{max} are the minimum and maximum photon energies in units of the beam energy, and the factor $Z(Z+1.35)$ accounts for the nuclear charge and approximates the atomic electrons; a typical cross section for carbon monoxide (CO) with large energy losses is a few barns.

Now, the number of scattered beam particles is

$$\frac{\Delta N}{N} = n_{gas} L \sigma_{brem}, \tag{35}$$

where L is the distance the beam travels, $n_{gas} = 3.2 \times 10^{22} P N_{atom}$ $\mathrm{m}^{-3}\,\mathrm{Torr}^{-1}$ at 300 K, P is the vacuum pressure, and N_{atom} is the number of atoms per molecule of gas. For example, assuming a pressure of 10 nTorr, in the 5-km-long Next Linear Collider beam delivery system, about 500 particles per train are lost due to bremsstrahlung. Of these, 20 are lost over the last 200 m before the interaction point (Reichel *et al.*, 1998).

A similar effect arises from inverse Compton scattering with thermal photons (Telnov, 1987). This process results in a large energy loss, which in turn can lead to a loss of the scattered particle. The scattering can be described with the parameter

$$x \equiv \frac{4E\omega\hbar}{m_e^2 c^4} \sin^2(\theta/2), \tag{36}$$

where E and $\hbar\omega$ are the beam and photon energies, m_e is the electron mass, and θ is the angle between the photon and the beam. The maximum energy of the scattered photon is

$$\hbar\omega'_{max} = \frac{x}{1+x} E \tag{37}$$

and, because the beam energy is much higher than the photon energy, a large fraction of the scattered photons are close to this maximum energy.

The photon density is described by the Planck blackbody formula

$$\frac{dn}{d\omega} = \frac{\omega^2}{\pi^2 c^3 (e^{\hbar\omega/kT} - 1)}, \tag{38}$$

with a total number of photons and an average photon energy of

$$n = 2 \times 10^7 T^3\,[\mathrm{K}^{-3}\,\mathrm{m}^{-3}] \quad \text{and} \quad \hbar\omega_{ave} = 2.7kT. \tag{39}$$

Unfortunately, to calculate the number of large-amplitude scatterings, the differential cross section needs to be integrated over θ and the photon density function, which must be done numerically. This and other scattering processes in the final focus can be studied with Monte Carlo simulations (Reichel *et al.*, 1998).

The effect can be roughly estimated by assuming that half the photons are scattered to the maximum energy, calculated from the average photon energy, and then multiplying the total photon density with the total Compton cross section, i.e.,

$$\frac{\Delta N}{N} = 0.5 n L \sigma_c, \tag{40}$$

where

$$\frac{\Delta E}{E} = \frac{x_{ave}}{1+x_{ave}} \quad \text{and} \quad x_{ave} = \frac{10.8EkT}{m_e^2 c^4}, \tag{41}$$

and the total Compton cross section is

$$\sigma_c = \frac{2\pi r_e^2}{x_{ave}} \left[\left(1 - \frac{4}{x_{ave}} - \frac{8}{x_{ave}^2}\right) \ln(1+x_{ave}) + \frac{1}{2} + \frac{8}{x_{ave}} - \frac{1}{2(1+x_{ave})^2}\right]. \tag{42}$$

For typical parameters, this expression tends to overestimate the number of large-amplitude scatterings by a factor of 2–5.

As an example, Monte Carlo simulations show that on average 50 particles per bunch train are lost in the 5-km Next Linear Collider beam delivery section, and two of these over the last 200 m (Reichel *et al.*, 1998).

Finally, we can calculate the effect of elastic Coulomb collisions. Here, the incident particles can scatter off the nucleus or the atomic electrons. In the former case, the energy change of the incident particle is relatively small and the primary effect is an angular deflection that may cause the particle to exceed the beam-pipe aperture. In comparison, the energy change can be significant when scattering is off the atomic electrons.

The differential cross section for Coulomb scattering on atomic nuclei can be written

$$\frac{d\sigma_{en}}{d\Omega} = \frac{4F^2(q) Z^2 r_e^2}{\gamma^2} \frac{1}{(\theta^2 + \theta_{min}^2)^2}, \tag{43}$$

where θ_{min} is a function of the screening due to the atomic electrons and is $\theta_{min} \approx \hbar/pa$, where p is the incident-particle momentum and a is the atomic radius: $a \approx 1.4 \lambda\!\!\!^{-}_e/\alpha Z^{1/3}$. In addition, $F(q)$ is the nuclear form factor, which for relatively small scattering angles can be approximated by 1, and we have neglected the recoil of the nucleus; both of these latter effects will reduce the large-angle scattering and will cause us to slightly overestimate the particle loss.

Assuming that the aperture is limited at a single location, such as the final doublet, the number of particles scattered to an amplitude greater than the aperture is

$$\frac{\Delta N}{N} = n_{gas} L \, \frac{2\pi Z^2 r_e^2}{\gamma^2 b^2} \int ds (R_{12}^2 + R_{34}^2), \tag{44}$$

where b is the limiting radius, R_{12} and R_{34} are the transfer matrix elements from the scattering position to the aperture, and we have assumed that $b^2 \gg (R_{12}^2 + R_{34}^2)\,\theta_{min}^2$.

According to Monte Carlo simulations, in the 5-km Next Linear Collider beam delivery system at a pressure of 10 nTorr, about 1000 particles per bunch train are lost due to hard Coulomb scattering, but only about 10 of these over the last 200 m (Reichel *et al.*, 1998).

Next we can calculate the elastic scattering from atomic electrons. Here, the angular deflection can be accounted for by replacing Z^2 with $Z(Z+1)$ in Eq. (44); this will overestimate the scattering but is a small correction anyway. However, as we have mentioned, in this case the recoil of the electron cannot be neglected and can result in a significant energy change to the incident particle. The differential cross section for a relative energy change of δ is

$$\frac{d\sigma_{ee}}{d\delta} = \frac{2\pi Z r_e^2}{\gamma} \frac{1}{\delta^2}, \tag{45}$$

and the number of particles scattered beyond a limiting energy aperture δ_{min} is

$$\frac{\Delta N}{N} = n_{gas} L \, \frac{2\pi Z r_e^2}{\gamma} \frac{1}{\delta_{min}}. \tag{46}$$

For the Next Linear Collider, this amounts to fewer than one lost particle per bunch train and is a negligible effect (Reichel *et al.*, 1998).

X. TOLERANCES

In this section, we shall discuss tolerances on the elements in the FFS. However, we should note that it is impossible to separate the tolerances from the tuning procedures (briefly discussed in the next section). For example, to calculate the amount of dispersion generated by moving a quadrupole, we must also know where the resulting trajectory oscillation is corrected. In the following, we shall neglect the tuning and simply calculate "bare" tolerances, but it should be emphasized that these are frequently unrealistically tight. To further simplify the discussion, we shall consider only effects that contribute to the vertical spot size, since these tolerances are usually significantly more stringent than those in the horizontal plane. Finally, we shall discuss only the effects or sensitivities of the elements; the final design tolerances must be determined so as to limit the total dilution and require balancing the difficulty with the sensitivities.

A. Incoming beam

If the geometric aberrations in the FFS are well corrected, the nonlinear aberrations will not be very sensitive to incoming betatron oscillations or changes in the incoming beam emittance. The $-I$ transformations in the CCX and CCY will cause most aberrations to cancel. However, synchrotron radiation in the quadrupoles, and especially the final doublet (Sec. VII), can impose severe constraints on the incoming trajectory jitter.

B. Trajectory errors

The dominant source of vertical trajectory errors is movements of the quadrupoles and rolls of the horizontal bending magnets (by roll we mean a rotation in the transverse plane, resulting in a nonzero horizontal dipole field component, causing vertical deflection). The position at the interaction point is simply given by the R_{34} transport matrix element from the element to the interaction point times the deflecting angle:

$$\Delta y^\star = y_q \int ds K_1 R_{34} \quad \text{and} \quad \Delta y^\star = \theta_b \int ds G R_{34}, \tag{47}$$

where y_q and θ_b are the quadrupole offset and the bending magnet roll.

Assuming that the optical functions vary slowly along the magnet, these expressions can be written in the simpler form

$$\frac{\Delta y^\star}{\sigma_y^\star} = y_q k_1 \sqrt{\frac{\beta_y}{\epsilon_y}} \, |\sin(\psi_y^\star - \psi_y)| \tag{48}$$

and

$$\frac{\Delta y^\star}{\sigma_y^\star} = \theta_b \Theta_b \sqrt{\frac{\beta_y}{\epsilon_y}} \, |\sin(\psi_y^\star - \psi_y)|, \tag{49}$$

where k_1 is the integrated normalized quadrupole strength, Θ_b is the bending angle of the bending magnet, β_y is evaluated at the magnet, and, for most magnets in the FFS, $|\sin(\psi_y^\star - \psi_y)| \approx 1$. The terms ψ_y^* and ψ_y denote the vertical betatron phases at the interaction point and at the location of the magnet, respectively (the betatron phase advance ψ characterizes the evolution of transverse trajectory oscillations along the beam line; it is intimately related to the beta function via $d\psi/ds = 1/\beta$). In subsequent sections, we shall present the sensitivities in terms of the transport matrix elements, which is convenient for calculations, but it is straightforward to transform them into this more intuitive form.

The tightest quadrupole sensitivity is almost always that on the final doublet, where, assuming that the doublet moves as a unit, the trajectory motion at the interaction point is roughly equal to the motion of the magnets. The sensitivity is even tighter for an asymmetric motion, where the horizontally and vertically focusing final magnets move in opposite directions. Fortunately most of the motion of the magnets in the FFS will be driven by ground motion, which tends to be correlated over long distances. In this case, the sensitivities are greatly relaxed because the deflections cancel naturally (Juravlev *et al.*, 1993; Zhuravlev *et al.*, 1995; Irwin *et al.*, 1996).

C. Dispersion

In the same manner as for the trajectory, we can estimate the dispersion generated by deflections. Here, two effects contribute: the chromatic dependence of the deflection and the chromatic dependence of the displaced downstream trajectory:

$$\Delta\sigma_y^\star = y_q k_1 \sigma_\epsilon |R_{34} - T_{346}|$$

and

$$\Delta\sigma_y^\star = \theta_b \Theta_b \sigma_\epsilon |R_{34} - T_{346}|, \tag{50}$$

where σ_ϵ is the rms energy spread and T_{346} is the second-order transport element (Brown, 1968), which will dominate downstream of the CCY because of the uncorrected vertical chromaticity (the T_{346} matrix element describes the second-order contribution to the shift in vertical interaction point position $\Delta y^\star$, caused by a simultaneous change in relative energy $\Delta\delta$ and slope $\Delta y'$ via $\Delta y^\star = R_{34}\Delta y' + R_{36}\Delta\delta + T_{346}\Delta\delta\Delta y' + \cdots$, where the coefficients R_{34} and R_{36} are the first-order transport-matrix elements).

Vertical dispersion can also be generated by rolls of the quadrupole magnets or displacements of the sextupole magnets:

$$\Delta\sigma_y^\star = 2\,\theta_q \eta_x k_1 \sigma_\epsilon |R_{34}| \quad \text{and} \quad \Delta\sigma_y^\star = y_s \eta_x k_2 \sigma_\epsilon |R_{34}|, \tag{51}$$

where η_x is the horizontal dispersion evaluated at the magnet and θ_q and y_s are the roll of the quadrupole and offset of the sextupole magnets.

D. Skew coupling

Skew coupling is generated by direct skew fields or by trajectory errors that cause offsets in the sextupoles. The direct skew fields arise from the detector solenoid as well as rolls of the quadrupole magnets or displacements of the sextupole magnets. In this case,

$$\Delta\sigma_y^\star = 2\,\theta_q k_1 \sigma_x |R_{34}| \quad \text{and} \quad \Delta\sigma_y^\star = y_s k_2 \sigma_x |R_{34}|, \tag{52}$$

where σ_x is the horizontal beam size at the magnet; the tightest roll tolerances are usually found for the final-doublet magnets. Of course, the FFS must be designed with tuning elements to correct for the skew coupling, since it is part of the design optics and is introduced by the detector solenoid. Fortunately, with flat beams, the skew correction needs to be applied only to the two phases that enlarge the vertical beam size at the interaction point, i.e., the $x^\star$-$y^\star$ and $x'^\star$-$y^\star$ terms, since the sensitivities for the horizontal beam size are much looser.

Another source of coupling is trajectory errors that displace the beam in one of the paired sextupoles of the CCX or CCY; because the sextupoles are separated by a $-I$ transformation, an oscillation passing through both magnets will have little effect, but an offset in one of the magnets can have a large effect. Hence this introduces additional sensitivities for the magnets inside the CCX or CCY:

$$\Delta\sigma_y^\star = \theta_b \Theta_b |R_{34b\to s}| k_2 \sigma_x |R_{34s\to\star}| \tag{53}$$

and

$$\Delta\sigma_y^\star = y_q k_1 |R_{34q\to s}| k_2 \sigma_x |R_{34s\to\star}|, \tag{54}$$

where $R_{34b\to s}$ and $R_{34s\to\star}$ are the transport matrix elements from the bending magnet to the sextupole, where the trajectory is offset, and then from the sextupole to the interaction point. Because of the strong focusing in the CCX and CCY, small errors can result in large trajectory offsets at the sextupoles, and this can be one of the more severe sensitivities.

XI. TUNING

In the FFS most important high-order aberrations are minimized by design, and the tolerances on the accuracy of their cancellations are relatively loose. However, the tolerances on the low-order aberrations are much tighter, and thus tuning strategies must be developed to minimize these aberrations routinely. For example, it is thought that in the Next Linear Collider FFS (Raubenheimer *et al.*, 1996; Zimmermann *et al.*, 1997), the first-order aberrations, such as dispersion and interaction-point waist position, will probably need to be tuned on an hourly basis, while the second-order and third-order aberrations, such as chromaticity and second-order dispersion, will need weekly to monthly tuning, and the fourth-order aberrations can be neglected.

To prevent luminosity loss, the tuning procedures must be designed to use orthogonal corrections for fast convergence to the optimal solutions (Walker *et al.*, 1993). Simulation tools have been found to be very effective for testing the procedures at the SLC (Woodley, 1994), and more recently the MERLIN code (Walker, 1997) was developed as part of the TESLA project (Brinkmann *et al.*, 1997).

Finally, the tuning procedures, which are usually based on beam-size measurements, are very sensitive to the accuracy of the measurements. It is presently thought that imperfect spot size measurements during the tuning of the low-order aberrations in the SLC were causing a 20–30 % luminosity loss until the 1997 SLC run (Emma *et al.*, 1997). Thus very accurate diagnostics are essential for the FFS. To alleviate this problem, the SLC FFS is now being tuned using dither feedback systems based on measurements of the energy loss due to beamstrahlung as described by Emma *et al.* (1997), with roughly an order-of-magnitude improvement in the tuning efficiency (Hendrickson *et al.*, 1997).

XII. OPTIMIZATION

The aberrations in a final-focus system as well as the effect of errors on the spot size can be analyzed using Lie-algebra techniques (Roy, 1992; Irwin, 1990), advanced software tools that combine Lie algebra with truncated-power-series algebra and particle tracking—for example, the programs DESPOT (Forest, 1997) or LEGO (Cai *et al.*, 1997), or more conventional element-to-element multiparticle tracking codes such as TURTLE (Brown and Iselin, 1974) or DIMAD (Servranckx *et al.*, 1990). DIMAD includes the effect of synchrotron radiation in bending magnets and quadrupoles (Roy, 1990). Specific automatic design and analysis programs for generic final-focus systems have also been developed—for example, the codes FFADA (Dunham and Napoly, 1994) and LCOPT (Yokoya, 1997).

XIII. ADVANCED DEVELOPMENTS

Several novel techniques have been proposed to overcome some of the design limitations of "conventional" final-focus systems. One important characteristic of an FFS is its momentum bandwidth. In most present-generation final-focus systems, using separate CCX and CCY sections, the bandwidth is typically limited by the chromatic breakdown of the $-I$ transform between sextupole pairs. This gives rise to fifth-order chromatic and chromogeometric terms such as those described by the Lie generators $p_x p_y^2 \delta^2$ and $p_y^2 \delta^3$. The bandwidth can be improved by introducing additional sextupoles (Brinkmann, 1990) in the final transformer and in the chromatic correction section and/or by an odd-dispersion optics, where the dispersion at the first sextupole is zero or of opposite sign to the second sextupole (Oide, 1992). While the odd-dispersion optics minimizes the term $p_x p_y^2 \delta^2$ (Oide, 1992), the additional sextupoles can also be employed to reduce the third-order chromaticity (generator $p_y^2 \delta^3$; Raubenheimer *et al.*, 1996). Most of the fifth-order aberrations decrease with increasing dispersion at the sextupoles.

Another technique, referred to as a *traveling focus* (Balakin, 1992), might be used to avoid luminosity reduction due to the depth of focus [Eq. (7)], which can be significant when $\sigma_z \geqslant \beta^*$. Here, the optical focal point is varied depending on the longitudinal position within the bunch. Particles in the head are focused at the actual interaction point. As the collision progresses, the focal points of both beams are shifted gradually backwards in longitudinal position, such that particles in the later parts of the bunches are focused at a point where they first come into contact with the opposing beam. The ensuing pinch effect then sustains a small spot size throughout the entire collision process. A traveling focus can be implemented either using uncorrected chromaticity and an energy-position correlation across the bunch or with a fast rf quadrupole.

Another problem is the length of a conventional FFS, which already at a beam energy of 1.5 TeV can occupy a significant fraction of the collider. In scaling to higher energies, the FFS length should increase rapidly with the energy (Zimmermann *et al.*, 1995). Assuming that (1) the beta functions decrease inversely with the beam energy, (2) the normalized emittances and the free length from the interaction point are held constant, and (3) the total length of the final-focus system is determined by synchrotron radiation in the bending magnets and by magnet position tolerances, the length of the FFS would increase as $\sim\gamma^2$. Different assumptions could imply a slightly weaker growth $\sim\gamma^{3/2}$ (Irwin, 1997) or $\sim\gamma$; however, the length increase is significant in all cases.

The final-focus length is determined to a large extent by its natural chromaticity, which in turn depends on the strength of the final quadrupoles and their proximity to the interaction point. Strong lenses very close to the interaction point would allow a significant reduction of the system length. Plasma lenses have been suggested as one tool to provide strong focusing near the interaction point. If a plasma is placed just in front of the interaction point, the beta function at the interaction point is reduced to (Chen *et al.*, 1993, 1996)

$$\frac{\beta^*_{x,y}}{\beta^*_{0,x,y}} = \frac{1}{1 + K\beta^*_{0,x,y}\overline{\beta}_{x,y}}, \tag{55}$$

where $K \approx 2\pi r_e n_p/\gamma$ (n_p is the plasma density) denotes the quadrupole gradient of the plasma lens, $\beta^*_{0,x,y}$ the horizontal (vertical) interaction-point beta function without the plasma lens, and $\overline{\beta}_{x,y}$ the beta function at the entrance to a lens of thickness d:

$$\overline{\beta}_{x,y} = \beta^*_{0,x,y}\left(1 + \left(\frac{d}{\beta^*_{0,x,y}}\right)^2\right). \tag{56}$$

Unfortunately this technique works best for electron beams. Positron beams respond very differently to a plasma lens and, although it is not impossible to focus a positron beam with a plasma, such focusing will introduce strong optical aberrations (Chen *et al.*, 1989).

If the plasma-density gradient is properly chosen, one can realize an adiabatic focusing lens that can bypass the Oide limit on the vertical spot size (Chen *et al.*, 1990). A new limit on the spot size arises from energy-loss considerations:

$$\sigma_q \geqslant (1.39\times10^{-8}\ \mathrm{m})\,\xi^2 \exp\left(-\frac{1.12}{\xi}\right), \tag{57}$$

where $\xi = (\gamma\epsilon_y/\epsilon_c)^{1/3}$ with $\epsilon_c \approx 6.2\ \mu$m.

Similarly, it may be possible to use the intense fields of demagnified low-energy bunches as a final lens. Here, the primary bunches collide with low-energy oppositely charged bunches a short distance from the interaction point. Also in this technique, referred to as *dynamic focusing*, the final lens, i.e., the low-energy bunches, is located close to the interaction point and thus the FFS chromaticity can be quite small. However, the pinch effect in the focusing collision would cause a luminosity loss (Irwin, 1997),

$$\frac{\Delta L}{L} \approx \frac{2}{15}\left(\frac{f_M \sigma_z}{f_Q \beta^*_M}\right)^2, \tag{58}$$

where $f_M = l^*$ is the focal length for the main beam, f_Q is the focal length of the lens beam, and β_M^* is the interaction-point beta function including the focusing effect from the lens beam. A rather short main-beam bunch length σ_z is required to avoid this luminosity loss.

Finally, a different approach, attractive for very-high-energy colliders, is to completely abandon the chromatic correction and to build a compact final focus consisting only of a few quadrupole lenses. This saves the space otherwise needed for the bending magnets, and thus considerably shortens the FFS. In addition, the tight tolerances on the relative alignment of beam orbit and sextupoles are eliminated. The disadvantage is that the absence of chromatic correction requires a very small incoming energy spread (Zimmermann and Whittum, 1997; Zimmermann, 1998).

ACKNOWLEDGMENTS

Many people have contributed to the advancements in linear-collider final-focus systems and to the present design philosophy. We had the pleasure to work with some of them, and would like to thank, in particular, R. Brinkmann, K. Brown, P. Chen, P. Emma, R. Helm, J. Irwin, O. Napoly, K. Oide, N. Walker, D. Whittum, and K. Yokoya for sharing their insights and for inspiring discussions. This work was supported by the Department of Energy under Contract No. DE-AC03-76SF00515.

REFERENCES

Akasaka, M., *et al.*, 1997, "JLC [Japanese Linear Collider] Design Study," KEK-REPORT 97-1.

Balakin, V., 1992, in *Proceedings of the International Workshop on Final Focus and Interaction Regions of Next Generation Linear Colliders*, SLAC-405 (SLAC, Stanford, CA), p. 178.

Balakin, V. E., and N. A. Solyak, 1986, in *Proceedings of the XIII International Conference on High Energy Accelerators*, Novosibirsk, USSR (Nauka, Novosibirsk, USSR), p. 146.

Berndt, M., *et al.*, 1991, "Final Focus Test Beam: Project Desion Report," SLAC-376 (SLAC, Stanford, CA).

Bethe, H., and J. Ashkin, 1953, in *Experimental Nuclear Physics*, Vol. 1, edited by E. Segre (Wiley, New York), p. 166.

Brinkmann, R., 1990, "Optimization of a Final Focus System for Large Momentum Bandwidth," DESY-M-90/14.

Brinkmann, R., 1993, in *Proceedings of the Fifth International Workshop on Next-Generation Linear Colliders*, Stanford, CA, SLAC-436 (SLAC, Stanford, CA), p. 363.

Brinkmann, R., G. Materlik, J. Rossbach, and A. Wagner, 1997, Eds., "Conceptual Design of a 500 GeV e^+e^- Linear Collider with Integrated X-ray Laser Facility," DESY 1997-048.

Brown, K. L., 1968, Adv. Part. Phys. **1**, 71.

Brown, K. L., and F. C. Iselin, 1974, "DECAY TURTLE (Trace Unlimited Rays Through Lumped Elements): A Computer Program for Simulating Charged Particle Beam Transport Systems, Including Decay Calculations," CERN-74-2.

Brown, K. L., and J. Spencer, 1981, in *Proceedings of the 1981 Particle Accelerator Conference*, Washington, D.C. (IEEE, Piscataway, NJ), p. 2568.

Cai, Y., *et al.*, "LEGO: A Modular Accelerator Design Code," in *Proceedings of the 1997 Particle Accelerator Conference*, Vancouver, Canada (IEEE, Piscataway, NJ), p. 2583.

Chen, P., 1993, "Disruption Effects from the Collision of Quasi-Flat Beams," in *1993 IEEE Particle Accelerator Conference*, Washington, D.C. (IEEE, Piscataway, NJ), p. 617.

Chen, P., C. K. Ng, and S. Rajagopalan, 1993, Phys. Rev. E **48**, 3022.

Chen, P., K. Oide, A. M. Sessler, and S. Yu, 1990, Part. Accel. **31**, 7.

Chen, P., S. Rajagopalan, and J. Rosenzweig, 1989, Phys. Rev. D **40**, 923.

Chen, P., A. Spitkovsky, and A. Weidemann, 1996, Int. J. Mod. Phys. A **11**, 1687.

Chen, P., and K. Yokoya, 1988a, Phys. Rev. D **38**, 987.

Chen, P., and K. Yokoya, 1988b, "Multibunch Crossing Instability," SLAC-PUB-4653.

Chen, P., and K. Yokoya, 1992, in *Frontiers of Particle Beams: Intensity Limitations*, Lecture Notes in Physics 400 (Springer-Verlag, Berlin), p. 415.

Dunham, B., and O. Napoly, 1994, "FFADA, Final Focus Automatic Design and Analysis," DAPNIA/SEA 94-06.

Emma, P., *et al.*, 1997, "Limitations of Interaction-point Spot-size Tuning at the SLC," in *Proceedings of the 1997 Particle Accelerator Conference*, Vancouver, Canada (IEEE, Piscataway, NJ), p. 452.

Forest, E., 1997, unpublished.

Hendrickson, L., *et al.*, 1997, "Luminosity Optimization Feedback in the SLC," in *Proceedings of the International Conference on Accelerator and Large Experimental Physics Control Systems* (Institute of High Energy Physics, Beijing, China).

Hertzbach, S. S., T. W. Markiewicz, T. Maruyama, and R. Messner, 1996, "Backgrounds at the Next Linear Collider," in *Snowmass 1996: New Directions for High-Energy Physics*, Snowmass, Colorado (SLAC, Stanford, CA), p. 178.

Hirata, K., B. Zotter, and K. Oide, 1989, Phys. Lett. B **224**, 437.

Hollebeek, R., 1981, Nucl. Instrum. Methods **184**, 333.

Irwin, J., 1990, Nucl. Instrum. Methods Phys. Res. A **298**, 460.

Irwin, J., *et al.*, 1996, "Ground Motion: Theory and Measurement," in *Zeroth Order Design Report for the Next Linear Collider*, edited by T. Raubenheimer *et al.*, LBNL-PUB-5424, SLAC-474, UCRL-ID-124161, p. 1044.

Irwin, J., 1997, "Dynamic Focusing Schemes for Linear Colliders," in *Proceedings of the 1997 Particle Accelerator Conference*, Vancouver, Canada (IEEE, Piscataway, NJ), p. 512.

Juravlev, V. M., *et al.*, 1993, "Investigations of Power and Spatial Correlation Characteristics of Seismic Vibrations in the CERN LEP Tunnel for Linear Collider Studies," CERN-SL-93-53.

Loew, G. A., 1995, Ed., "International Linear Collider Technical Review Committee Report," SLAC-R-95-471, with updates available at: http://www.slac.stanford.edu/xorg/ilc-trc/ilc-trchome.html.

Murray, J. J., K. L. Brown, and T. Fieguth, 1987, in *Proceedings of the 1987 IEEE Particle Accelerator Conference*, Washington, D.C. (IEEE, Piscataway, NJ), p. 1331.

Myers, S., 1995, in *Proceedings of the IEEE Particle Accelerator Conference*, Dallas, Texas (IEEE, Piscataway, NJ), p. 476.

Oide, K., 1988, Phys. Rev. Lett. **61**, 1713.

Oide, K., 1992, in *Proceedings of the 15th International Conference on High Energy Accelerators*, Hamburg, Germany (World Scientific, River Edge, NJ), p. 861.

Palmer, R., 1988, in *Snowmass DPF Summer Study 1988: High Energy Physics in the 1990's*, Snowmass, Colorado (World Scientific, NJ), p. 613.

Raubenheimer, T., and F. Zimmermann, 1996, SLAC internal report, NLC-Note-23, unpublished.

Raubenheimer, T., *et al.*, 1996, Eds., Zeroth Order Design Report for the Next Linear Collider, 1996, LBNL-PUB-5424, SLAC-474, UCRL-ID-124161.

Reichel, I., *et al.*, 1998, in *Proceedings of the 1998 International Computational Accelerator Physics Conference (ICAP'98)*, Monterey, California (forthcoming).

Rosenzweig, J. B., B. Autin, and P. Chen, 1989, in *Proceedings of the 1989 Lake Arrowhead Workshop on Advanced Accelerator Concepts* (AIP, New York), p. 324.

Rosenzweig, J. B., and P. Chen, 1991, in *Proceedings of the 1991 IEEE Particle Accelerator Conference*, San Francisco (IEEE, Piscataway, NJ), p. 3225.

Roy, G., 1990, Nucl. Instrum. Methods Phys. Res. A **298**, 128.

Roy, G., 1992, Ph.D. thesis, Stanford University, SLAC-397.

Sands, M., 1979, "The Physics of Electron Storage Rings," SLAC-121.

Sands, M., 1985, "Emittance Growth from Radiation Fluctuations," SLAC AP-47, unpublished.

Seeman, J., 1990, Annu. Rev. Nucl. Part. Sci. **41**, 389.

Servranckx, R., *et al.*, 1990, "User's Guide to the Program DIMAD," SLAC-0285.

Telnov, V., 1987, Nucl. Instrum. Methods Phys. Res. A **260**, 304.

Walker, N., 1997, "MERLIN," presented at Linear Collider 97 workshop, Dubna, Russia, unpublished.

Walker, N., *et al.*, 1993, "Global Tuning Knobs for the SLC Final Focus," in *Proceedings of the 1993 Particle Accelerator Conference*, Washington, D.C. (IEEE, NJ), p. 95.

Whittum, D. H., A. M. Sessler, J. J. Stewart, and S. S. Yu, 1990, Part. Accel. **34**, 89.

Woodley, M., 1994, private communication.

Yokoya, K., 1988, "Impedance of Slowly Tapered Structures," CERN SL/90-88.

Yokoya, K., 1997, private communication.

Zhuravlev, V. M., *et al.*, 1995, "Seismic Conditions in Finland and Stability Requirements for the Future Linear Collider," e-print HU-SEFT-R-1995-01.

Zimmermann F., 1998, in *Proceedings of the 8th Workshop on Advanced Accelerator Concepts*, Baltimore, Maryland (AIP, New York), p. 103.

Zimmermann, F., R. Helm, and J. Irwin, 1995, "Optimization of the Next Linear Collider Final Focus System," in *Proceedings of the 1995 Particle Accelerator Conference*, Dallas, Texas (IEEE, New York), p. 710.

Zimmermann F., and D. H. Whittum, 1997, in *Proceedings of the 2nd International Workshop on Electron-Electron Interactions at TeV Energies*, Santa Cruz, California, 1997; Published in Int. J. Mod. Phys. A **13**, 2525.

Zimmermann, F., *et al.*, 1996, "Collimator Wake Fields in the SLC Final Focus," in *Proceedings of the Fifth European Particle Accelerator Conference*, Sitges, Spain (Inst. Physics, Bristol, UK), p. 504.

Zimmermann, F., *et al.*, 1997, "Performance Issues, Downtime Recovery and Tuning in the Next Linear Collider (NLC)," in *Proceedings of the 1997 Particle Accelerator Conference*, Vancouver, Canada (IEEE, Piscataway, NJ), p. 608.